Neutron-skin thickness determines the surface tension of a compressible nuclear droplet

W. Horiuchi,[1] S. Ebata,[2] and K. Iida[3]
[1]*Department of Physics, Hokkaido University, Sapporo 060-0810, Japan*
[2]*Nuclear Reaction Data Centre, Faculty of Science, Hokkaido University, Sapporo 060-0810, Japan*
[3]*Department of Mathematics and Physics, Kochi University, Kochi 780-8520, Japan*
(Received 14 July 2017; revised manuscript received 31 August 2017; published 22 September 2017)

We systematically investigate the neutron-skin thickness of neutron-rich nuclei within a compressible droplet model, which includes several parameters characterizing the surface tension and the equation of state (EOS) of asymmetric nuclear matter as well as corrections due to the surface diffuseness. Such a systematic analysis helps towards constraining the EOS parameters of asymmetric nuclear matter and the poorly known density dependence of the surface tension; the latter is estimated with help of available experimental data for the neutron and proton density distributions and the nuclear masses. Validity of the present approach is confirmed by calculating realistic density distributions of Ca, Ni, Zr, Sn, Yb, and Pb isotopes within a microscopic Skyrme-Hartree-Fock+BCS method for various sets of the effective nuclear force. Our macroscopic model accompanied by the diffuseness corrections works well in the sense that it well reproduces the evolution of the microscopically deduced neutron-skin thickness with respect to the neutron number for selected sets of the effective nuclear force. We find that the surface tension of the compressible nuclear droplet is a key to bridging a gap between microscopic and macroscopic approaches.

DOI: 10.1103/PhysRevC.96.035804

I. INTRODUCTION

Constraining the parameters that characterize the equation of state (EOS) of asymmetric nuclear matter from empirical data for laboratory nuclei is one of the possible approaches to the EOS. However, the EOS parameters are still uncertain partly because a significant fraction of nucleons lie in the surface region of a nucleus and partly because empirical data for neutron-rich unstable nuclei are hard to obtain accurately. For example, traditional electron elastic scattering measurements have revealed that saturation of the density holds for stable nuclei. Since experimental data are limited for such short-lived unstable nuclei, even the systematics of neutron and proton radii has not been established yet. In fact, hundreds of theoretical models, which equally well describe the saturation of the density and binding energy of stable nuclei, provide different EOS parameter sets (see, for example, Ref. [1]).

Astrophysical constraints on the EOS parameters might be relevant, e.g., thanks to the recent precise mass measurement of a massive neutron star [2], but such constraints would be influenced by the poorly known EOS of neutron star matter at supranuclear densities. It is thus still reasonable to focus on nuclear observables that are sensitive to the symmetry energy at subnuclear densities. One of such observables is neutron-skin thickness, which is defined by difference between root-mean-square (rms) point-neutron and point-proton radii. In fact, a relationship between the symmetry energy and the neutron-skin thickness has actively been discussed by several theoretical works [3–8].

For stable nuclei, the charge-density distributions are well determined from electron elastic scattering [9]. To determine the point-neutron radius experimentally, a parity-violating electron scattering experiment was recently performed for ^{208}Pb [10]. Uncertainty in the resultant neutron-skin thickness is relatively large, although a further experiment is being planned to achieve higher precision [11]. We thus focus on proton elastic scattering experiments [12,13], which allow one to extract the neutron radius from the overall fit of the differential cross sections up to the backward angles where the data are fairly sensitive to the elusive inner regime. The experiments provide reliable data for the neutron-skin thickness of stable Pb and Sn isotopes. For unstable nuclei, we remark that the total reaction cross section on a proton target has been used to extract a neutron tail of halo nuclei (see, for example, Refs. [14,15]), and is suggested as a promising tool to extract the neutron-skin thickness [16,17]. A combination of the total reaction and charge-changing cross section measurements is also utilized for this purpose with use of a carbon target [18–21].

Theoretically, many nonrelativistic and relativistic models for the effective nuclear force have been proposed in such a way as to reproduce the saturation properties of stable nuclei, while each model corresponds to a particular set of the EOS parameters. Classification of the models in terms of the EOS parameters is useful because such parameters are available for any form of the nuclear Hamiltonian. Among others, the Skyrme type Hamiltonian has more than a hundred versions that give different sets of the EOS parameters through Skyrme-energy-density functional (Skyrme-EDF) calculations [1]. In Ref. [22], Brown selected sound Skyrme-EDF models by making use of the neutron-skin thickness of doubly magic nuclei as a constraint on the EOS parameters. However, uncertainty in the EOS parameters, particularly the slope parameter of the symmetry energy, L, is still large. As mentioned above, this comes from the fact that many nucleons are present at around the nuclear surface. It would thus be significant to consider a relationship between the nuclear surface and the EOS parameters.

For this purpose, we take a macroscopic approach to the neutron-skin thickness based on a compressible droplet model [23]. This model does not depend on details of the nuclear

Hamiltonian, but its underlying physics is the thermodynamics alone. Traditionally, a nuclear droplet model is formulated by assuming that the droplet is incompressible, but the nuclear density is not strictly saturated in finite nuclei. In fact, the nuclear droplet has to be compressible. In the compressible droplet model, the surface tension depends generally on the density in the nuclear interior, while mechanical equilibrium determines the optimal value of the internal density [24]. In the case of neutron-rich nuclei in which nonzero neutron excess generally occurs in the nuclear interior even in the presence of the neutron skin, the optimal density in the interior is primarily controlled by L through the saturation density of bulk matter that has the same neutron excess. Then, the thermodynamics of the surface dictates the neutron-skin thickness of neutron-rich nuclei to have an explicit dependence on L via the density dependence of the surface tension. This is because the neutron skin, a manifestation of adsorption of excess neutrons onto the nuclear surface, is thermodynamically related to the shift of the surface tension due to a quasistatic change in the neutron excess in the nuclear interior.

Whereas the compressible droplet model roughly explains the neutron-skin thickness of stable nuclei, corrections that originate from surface diffuseness of the nuclei should be carefully taken into account to extract the bulk properties of nuclear matter. Generally, such corrections, i.e., the surface width difference between neutrons and protons, are not considered, although they can have non-negligible effect [25]. When one considers more neutron-rich nuclei, the effect has to be more significant because the difference in the Fermi level between protons and neutrons becomes larger. Since the density dependence of the surface tension of the nuclear droplet is poorly known, furthermore, theoretical uncertainties are too large to constrain the EOS parameters [23].

In this paper, we revisit the expression for neutron-skin thickness within a compressible droplet model proposed in Ref. [23] and extend it by adding surface diffuseness corrections between neutrons and protons. For several sets of the EOS parameters that correspond to the Skyrme effective interactions adopted here, we determine the density dependence of the surface tension of the nuclear droplet in such a way that the expression for the neutron-skin thickness is consistent with empirical data for the neutron and proton density distributions of stable Sn and Pb isotopes. We then utilize the microscopic Skyrme-EDF method to calculate realistic density distributions of Ca, Ni, Zr, Sn, Yb, and Pb isotopes, as well as the EOS parameters. We finally compare the neutron-skin thickness of Ca–Pb isotopes that can be calculated from the macroscopic expression by using the determined density dependence of the surface tension with the results directly evaluated from the microscopic Skyrme-EDF calculations. We find that whether they agree well with each other or not depends on the adopted effective nuclear force. This result opens a way to further constrain the EOS parameters.

In the next section, we give definitions of various quantities of interest and brief explanations of our macroscopic models. Section II A briefly explains a compressible droplet model. A relationship between the neutron-skin thickness and the EOS parameters is also given in terms of a primary factor that characterizes the neutron excess dependence of the neutron skin thickness. In Sec. II B, nuclear surface width correction to the droplet model expression for the neutron-skin thickness is introduced. We carefully define the nuclear surface width or diffuseness for general nuclear density distributions and use it for the correction. Section III presents our results and discussions. After brief explanation of how we obtain realistic density distributions by a microscopic nuclear mean-field model in Sec. III A, we present in Sec. III B the surface widths—obtained from realistic nuclear densities—which effectively describe the surface properties of neutrons and protons. Then, in Sec. III C, we determine the primary factor of the neutron-skin thickness in the droplet model by using available experimental data. This factor is correlated with the parameter χ that controls the density dependence of the surface tension of the nuclear droplet. Finally, a comparison of the microscopic theory and macroscopic droplet model is made in terms of evolution of the neutron-skin thickness with respect to neutron excess in Sec. III D. Some microscopic models are not thermodynamically favored because they fail in reproducing such evolution obtained by the macroscopic model and thus do not satisfy the thermodynamic properties of finite nuclear matter. Effects of the pairing interaction on the nuclear surface are also discussed in Sec. III E. Conclusions are given in Sec. IV.

II. MODELS

In this section we summarize basic features of our compressible droplet model for nuclei and apply it to a description of the neutron-skin thickness. We then add corrections due to the surface diffuseness.

A. Neutron-skin thickness in a compressible droplet model

1. Definitions

Let us consider an atomic nucleus, i.e., an A-nucleon system that consists of N neutrons and Z protons. Neutron-skin thickness of this system is defined as the difference between point-neutron and proton rms radii:

$$\Delta r_{np} = \langle r_n^2 \rangle^{\frac{1}{2}} - \langle r_p^2 \rangle^{\frac{1}{2}}. \tag{1}$$

These rms radii can be calculated by using the corresponding density distributions, $\rho_q(\boldsymbol{r})$, as

$$\langle r_q^2 \rangle = \frac{\int d\boldsymbol{r}\, r^2 \rho_q(\boldsymbol{r})}{\int d\boldsymbol{r}\, \rho_q(\boldsymbol{r})}, \tag{2}$$

where the subscript q takes p and n for protons and neutrons, respectively. It is noted that, in the case of a sphere with uniform density distribution, the sharp cutoff radius, R_q, is related to the rms radius by

$$R_q = \sqrt{\frac{5}{3}} \langle r_q^2 \rangle^{\frac{1}{2}}. \tag{3}$$

The point-nucleon (matter) rms radius is defined by

$$\langle r^2 \rangle^{\frac{1}{2}} = \left(\frac{N}{A} \langle r_n^2 \rangle + \frac{Z}{A} \langle r_p^2 \rangle \right)^{\frac{1}{2}}. \tag{4}$$

We can use the same definitions as given in Eqs. (2) and (3) for the matter radius and density, but we omit the subscript m for the sake of simplicity. As a measure of neutron excess, it is convenient to define the asymmetry parameter:

$$\delta = \frac{\rho_n - \rho_p}{\rho_n + \rho_p}. \tag{5}$$

Generally, δ is a function of $\boldsymbol{r}$, but we shall often take it as constant $\simeq (N-Z)/A$. This approximation is good when $R_n \simeq R_p$.

2. *Compressible droplet model*

We now give expression for the neutron-skin thickness in a compressible droplet model following Ref. [23]. In this model, a nucleus is viewed as a spherical liquid drop of variable uniform density ρ_q and sharp cutoff radius R_q. For nearly symmetric nuclei, which satisfies $R_n \simeq R_p$, one can ignore the neutron-skin thickness at first approximation. Then, the volume energy is A times the bulk energy per nucleon, w, which can be expressed in a form expanded with respect to the matter density and neutron excess around $\rho = \rho_0$ and $\delta = 0$ [26]:

$$w(\rho,\delta) = w_0 + \frac{K_0}{18\rho_0^2}(\rho-\rho_0)^2 + \left[S_0 + \frac{L}{3\rho_0}(\rho-\rho_0)\right]\delta^2, \tag{6}$$

where ρ_0 and w_0 are the saturation density and the energy of symmetric nuclear matter. K_0, S_0, and L are the so-called incompressibility of symmetric nuclear matter, the symmetry energy coefficient, and the density symmetry coefficient or slope parameter, respectively. Note that the saturation density of nearly symmetric nuclear matter can be obtained from Eq. (6) as $\rho_0(1 - 3L\delta^2/K_0)$. The surface energy is controlled by the density-dependent surface tension, σ, which can also be expanded as

$$\sigma(\rho,\delta) = \sigma_0\left(1 - C_{\rm sym}\delta^2 + \frac{\chi}{\rho_0}(\rho-\rho_0)\right), \tag{7}$$

where σ_0 is the surface tension at $\rho = \rho_0$ and $\delta = 0$, and $C_{\rm sym}$ is the surface symmetry energy coefficient. The parameter χ represents the density dependence of the surface tension defined by

$$\chi \equiv \frac{\rho_0}{\sigma_0}\frac{\partial\sigma}{\partial\rho}\bigg|_{\rho=\rho_0,\delta=0}. \tag{8}$$

In the compressible droplet model [23], a neutron skin arises from adsorption of excess neutrons onto the surface, which is in turn in thermodynamic equilibrium with the bulk system of A nucleons. By separating the bulk system into the skin and interior (neutron reservoir) regions, one can relate the neutron-skin thickness with the EOS and surface parameters introduced in Eqs. (6) and (7), respectively. For a given R_p, the neutron-skin thickness can be expressed up to leading order in δ by

$$\Delta r_{np}^{\rm vol} \simeq \sqrt{\frac{3}{5}}\left[C\left(\delta - \frac{Ze^2}{20R_pS_0}\right)\left(1+\frac{3C}{2R_p}\right)^{-1} - \frac{Ze^2}{70S_0}\right] \tag{9}$$

with a primary factor

$$C = \frac{2\sigma_0}{S_0\rho_0}\left(C_{\rm sym} + \frac{3L\chi}{K_0}\right). \tag{10}$$

Note that the depression of the neutron-skin thickness due to the Coulomb interaction is considered in the formula by the terms involving Z. The density dependence of the surface tension, χ, which is a key parameter of this work, is correlated with L and K_0 as well as $C_{\rm sym}$. So far the χ value is poorly known, but typically two values of χ are assumed: $\chi = 0$ in the absence of the density dependence [27] and $\chi = 4/3$ in the Fermi-gas model [28].

B. Diffuseness correction to neutron-skin thickness

Since the nuclear surface distribution is in general different for protons and neutrons, the surface width correction to the neutron-skin thickness occurs as the following term [25]:

$$\Delta r_{np}^{\rm surf} \simeq \sqrt{\frac{3}{5}}\frac{5}{2R}\left(b_n^2 - b_p^2\right), \tag{11}$$

where b_n (b_p) is the surface width of the neutron (proton) density. If the density profile is the Fermi-type distribution, $f(r) = \{1 + \exp[(r-\bar{R}_q)/a_q]\}^{-1}$, the quantity b_q can be related to the diffuseness parameter a_q by $b_q \sim \pi a_q/\sqrt{3}$. The b_n and b_p values are typically taken as $\sim$1 fm, which corresponds to the empirical diffuseness value of $\sim$0.54 fm [29].

In this work, we employ realistic density distributions that can be generated by a microscopic mean-field model, while we need a sound way of quantifying the surface width. Warda *et al.* introduced a convenient definition of the surface width for one-dimensional half-infinite nuclear matter in equilibrium with the vacuum [25]. Here we extend it to a three-dimensional finite nucleus. With a spherical density distribution, $\rho_q(r)$, and its derivative, $\rho_q'(r)$, we calculate the mean location of the surface, c_q, by

$$c_q = \frac{4\pi\int_0^\infty r^3\rho_q'(r)dr}{4\pi\int_0^\infty r^2\rho_q'(r)dr}. \tag{12}$$

The square of the surface width can then be evaluated from the mean-square radius of the gradient of the density distribution measured with reference to c_q as

$$b_q^2 = \frac{4\pi\int_0^\infty (r-c_q)^2r^2\rho_q'(r)dr}{4\pi\int_0^\infty r^2\rho_q'(r)dr}. \tag{13}$$

This definition is reasonable if the Fermi distribution well approximates $\rho_q(r)$. This is because b_q defined in Eq. (13) approaches $\pi a_q/\sqrt{3}$ for large radius parameter $\bar{R}_q$ when the Fermi distribution is employed. We remark that in the case of the trapezoidal distribution with the top-bottom length difference of D_q, it approaches $D_q/2\sqrt{3}$, which is significantly small for the empirical value of D_q of order 2.2 fm [30].

The Fermi distribution always gives an almost uniform distribution in the interior region of a nucleus, whereas any realistic density distribution exhibits some oscillatory behavior. The derivative of such a density distribution also oscillates and is not always small in the interior region. In some cases, therefore, b_q does not properly reflect the surface

width or surface diffuseness, but it contains appreciable effects coming, e.g., from the internal depression of the density. To avoid this problem, we assume that the surface diffuseness is symmetric at $r = c_q$ and employ only the outer region of the integrand:

$$b_q^2 = \frac{2\int_{c_q}^{\infty}(r-c_q)^2\left[(r-c_q)^2+c_q^2\right]\rho_q'(r)dr}{\int_0^{\infty} r^2\rho_q'(r)dr}. \qquad (14)$$

Note that the second term in the expansion of $r^2 = (r-c_q)^2 + 2c_q(r-c_q) + c_q^2$ is omitted by assuming that ρ_q' is symmetric with respect to $r = c_q$. When we adopt Eq. (14) for realistic density distributions, as expected, the values of b_q lie mostly between those of the trapezoidal and Fermi-type distributions. Hereafter we shall thus use the above definition for b_q unless otherwise mentioned. Note that Eq. (11) is derived by assuming that the nuclear matter has a flat interface as was formulated in Ref. [25], but this b_q defined here is for a three-dimensional density distribution that includes the curvature effect of the nuclear sphere. Since the effect is of higher order in the droplet model, we can ignore this difference for medium-heavy and heavy nuclei.

III. RESULTS AND DISCUSSIONS

In this section we present our calculations of the nuclear surface diffuseness based on the microscopic theory, determine the primary factor (10) that is consistent with empirical data for the neutron and proton distributions, check the consistency between the microscopic and macroscopic evaluations of the neutron-skin thickness, and finally discuss the pairing effect on the nuclear surface.

A. Density distributions with microscopic mean-field theory

Realistic density distributions of Ca, Ni, Zr, Sn, Yb, and Pb isotopes are generated by the Skyrme Hartree-Fock (HF) + BCS method in the three-dimensional coordinate space. We employ a constant monopole pairing as detailed in Refs. [31,32]. All details of the calculation are given in Refs. [17,33]. Since we do not assume any spatial symmetry in the calculation, the deformation effect, which changes the structure of the nuclear surface, is fully taken into account. The obtained intrinsic density is generally deformed, while the density distribution in the ground state is spherical in the laboratory frame. Such a spherical density distribution can be obtained by taking the angle average as was done in Ref. [34]. Validity of the resulting density distributions can be confirmed by comparison with experimental data in the following way. These density distributions, once build into an appropriate reaction theory based on the Glauber formalism [35], reproduce the total reaction cross sections [34,36] obtained by the recent measurements [37,38] within error bars.

The nuclear structure is somewhat sensitive to the Skyrme interaction employed. For example, the SkM* and SLy4 interactions give a different neutron number dependence of the nuclear radii since nuclear deformations change the density profiles at around the nuclear surface in a different manner [34]. To test the interaction model dependence, we employ SkM* [39], SLy4 [40], SkI3 [41], KDE0v1 [42], LNS [43], SkT1,2,3 [44], and SV-sym32 [45]. These Skyrme interactions except for SkI3 belong to those selected according to the classification suggested in Ref. [22].

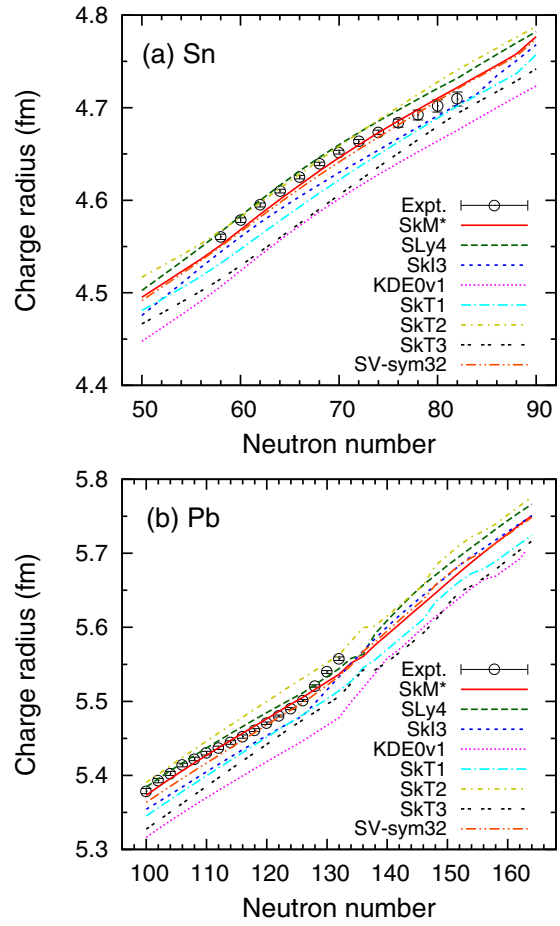

FIG. 1. Charge radii of (a) Sn and (b) Pb isotopes. The point-proton radii obtained by the HF+BCS proton density distributions are converted to the charge radius by taking into account finite size corrections of the proton and neutron charge radii and the Darwin-Foldy term [47]. The experimental charge radii are taken from Ref. [46].

To see the characteristics of the interactions, we compare, in Fig. 1, the calculated charge radii of Sn and Pb isotopes with experimental data [46]. The results with the LNS interaction are not plotted because the calculated charge radii are considerably smaller than those obtained with the other interactions by ∼0.1 fm. Though there are some quantitative differences, the results with the SkM*, SLy4, SkT2, and SV-sym32 interactions exhibit a fairly good agreement with the experimental charge radii, while the results with the SkI3, KDE0v1, SkT1, and SkT3 interactions deviate appreciably from the measured values. We remark that the SkI series which simulates the spin-orbit strength of the relativistic mean-field model can reproduce the kink [48]. In fact, the SkI3 interaction alone shows such a kink behavior at the neutron number 126 of Pb isotopes.

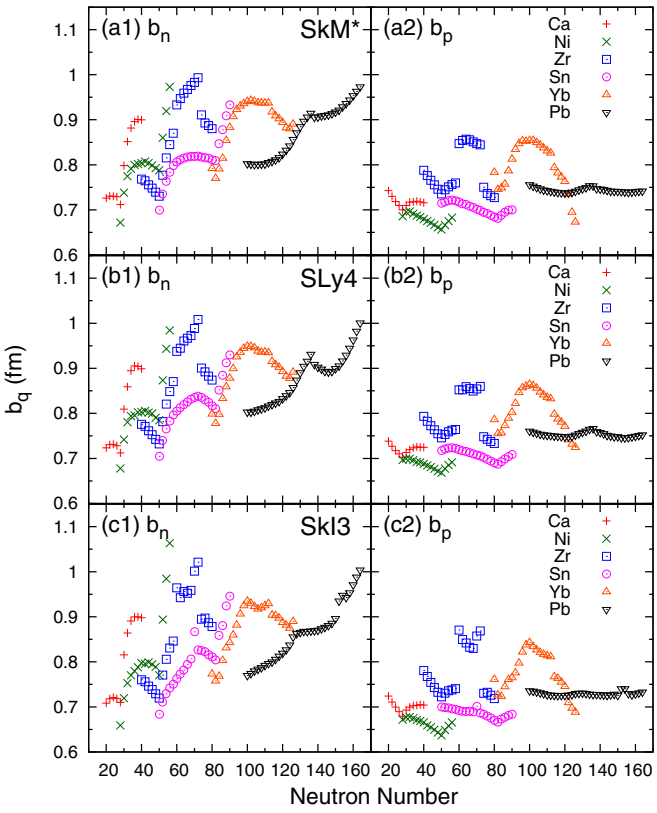

FIG. 2. Surface widths of Ca, Ni, Zr, Sn, Yb, and Pb isotopes extracted from the (left) neutron and (right) proton density distributions, respectively. For calculations of these distributions, the (a) SkM*, (b) SLy4, and (c) SkI3 interactions are employed from top to bottom, respectively.

B. Nuclear surface width

The nuclear surface has important information on the nuclear structure, such as deformation, skin, weakly-bound neutron orbits, etc. In fact, the nuclear deformation changes density profiles at the nuclear surface and enhances the nuclear size. Comparison of theoretical models with the total reaction cross section measurements supports strong deformations in the neutron-rich Ne and Mg isotopes [34,49–52], although whether or not this conclusion holds for any collision energy has yet to be clarified. The low-lying electric dipole ($E1$) strength is also sensitive to the nuclear surface. The abrupt change of the low-lying $E1$ strength at the magic numbers, which is possibly measured by the total reaction cross section with a heavy target nucleus [53], can be explained by the structure change of the outermost single-particle orbit [31].

It is interesting to see a systematic trend of the nuclear surface width of the HF+BCS densities. Figure 2 displays how the surface widths obtained for the proton and neutron densities of Ca, Ni, Zr, Sn, Yb, and Pb isotopes depend on the neutron number. These surface widths are found to range between $\sim$0.6 and $\sim$1 fm. Although there are some quantitative differences, all the Skyrme interactions show a similar neutron number dependence of the surface width. We remark that the value of b_q is generally smaller in the Thomas-Fermi calculations [25] in which the surface diffuseness tends to be underestimated [54].

Since the surface width is closely related to the diffuseness of the nuclear surface, the behavior of b_q exhibits some interesting nuclear structure properties. Generally, b_n increases as the Fermi level rises, which allows the outermost neutron orbit to extend and hence gives larger diffuseness at the nuclear surface. The behavior of b_q is different in a way that depends on the quantum number, particularly the angular momentum of the outermost neutron orbits. In fact, sudden rises are found at the spherical magic numbers, i.e., $N = 28$ for Ca, $N = 50$ for Ni, $N = 82$ for Sn, and $N = 126$ for Pb. A change of the major shell or angular momentum of the outermost single-particle orbit can be seen in b_n at the magic numbers. For Zr and Yb isotopes, the b_n becomes maximum in the open-shell regime between the magic numbers because the density distribution at the nuclear surface extends due to the nuclear deformation.

It is interesting to note that b_p tends to decrease with neutron number, a tendency that stems from the fact that, in general, the proton Fermi level becomes deeper with increasing neutron number. Thus, in neutron-rich unstable nuclei, the proton density distribution at the nuclear surface is significantly sharp as compared with the neutron one. The local maxima and minima of b_p arise basically by following the behavior of b_n. This is natural because the interaction between protons and neutrons is strongly attractive and hence they tend to be close to each other.

C. Primary factor that expresses the neutron-skin thickness in a compressible droplet model

Here we propose a way to determine the unknown parameter in the compressible droplet model from the existing experimental data. In fact, the precise measurements of intermediate energy, proton-elastic scattering cross sections have been performed for ^{116,118,120,122,124}Sn [12] and ^{204,206,208}Pb [13]. By combining these measurements with the proton density distributions extracted from the electron-scattering measurements [9], the neutron density distributions and thus the neutron-skin thickness have been extracted.

Within our model, the neutron skin thickness can be expressed as a sum of the volume and surface terms given by Eqs. (9) and (11): $\Delta r_{np} = \Delta r_{np}^{\rm vol} + \Delta r_{np}^{\rm surf}$. We determine R_p, R, b_n, and b_p from the empirical proton and neutron density distributions [12,13] and then substitute the resultant values into the expressions for $\Delta r_{np}^{\rm vol}$ and $\Delta r_{np}^{\rm surf}$. Aside from S_0, which will be discussed just below, the volume term still contains one unknown factor, namely, C, Eq. (10), which roughly determines a slope of $\Delta r_{np}^{\rm vol}$ with respect to δ. We can thus fix the factor C in such a way as to minimize the rms deviation from the empirical neutron-skin thickness as defined by $\sqrt{\frac{1}{N_d}\sum_{i=1}^{N_d}[\Delta r_{np}(i) - \Delta r_{np}^{\rm Expt.}(i)]^2}$, where N_d denotes the number of available data.

Figure 3 displays the theoretical and experimental Δr_{np} for stable Sn and Pb isotopes. Given phenomenological estimates of the symmetry energy coefficient, $S_0 = 32 \pm 4$ MeV [54], we obtain $C = 1.06^{+0.08}_{-0.07}$ and find that uncertainty in C that comes from the error ± 4 MeV of S_0 is much smaller than that from the

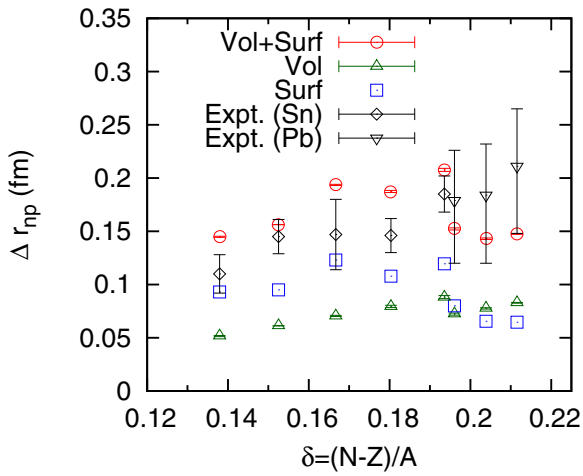

FIG. 3. Neutron-skin thickness (circles) calculated for Sn and Pb isotopes within the compressible droplet model using the empirical density distributions [12,13]. Decomposition into the volume (triangles) and surface (squares) terms and the empirical skin-thickness values (inverted triangles for Pb; diamonds for Sn) are also given. Error bars of the total neutron-skin thickness and its volume contribution indicate a range of the calculated values with $S_0 = 28$–36 MeV.

experimental uncertainty [12,13]. This means that the results for C are dictated by the measurements, irrespective of the assumed values of the EOS and surface parameters. We neglect uncertainties in the surface term, which come partly from unpublished uncertainties in the deduced neutron and proton density distributions. Another factor is the shell and pairing effects, which modify the nuclear surface profile and are effectively included in the surface term of Eq. (11), as will be discussed in Sec. III E. Judging from Fig. 3, however, we note that those effects have to be also included in the volume term or C in such a way that C is smaller (larger) for Sn (Pb) isotopes than the above value, but remain to be examined in the present qualitative analysis. For better estimates of C, it would be significant to increase the number of empirical data for the proton and neutron density distributions of neutron-rich nuclei. In the next subsection, we will discuss the validity of the obtained C by using the microscopic HF+BCS model calculations.

D. Comparison of the neutron-skin thickness between the macroscopic and microscopic models

Here we show usefulness of our macroscopic formula for the neutron-skin thickness by comparing it with the skin thickness obtained by the Skyrme-HF+BCS model. The EOS parameters predicted by hundreds of the Skyrme interactions within the HF framework are available in Ref. [1], where, for a given Skyrme parameter set, the corresponding EOS parameters are listed.

First, we redetermine C by the same procedure as described in the previous subsection but for the S_0 value that corresponds to the given Skyrme-EDF. Although this value ranges approximately from 30 to 35 MeV, the S_0 dependence of C is tiny, as shown above, and hence the redetermined value of C lies in the range of C as obtained above from stable Sn and Pb isotopes. We can then fix the unknown parameter in the compressible droplet model (10), namely, the density dependence of the surface tension, χ. Here we set the values of σ_0 and $C_{\rm sym}$ to be 1 MeV fm^{-2} and 1.9, respectively, which are determined by the global fit of experimental nuclear masses within the framework of the incompressible droplet model [55]. This is reasonable because each effective interaction is constructed in such a way as to reproduce the same measured masses of stable nuclei. Note, however, that there are uncertainties in the above values of σ_0 and $C_{\rm sym}$. Even in the incompressible limit, $C_{\rm sym}$ is uncertain, as will be shown below in the present subsection. Once the effect of finite compressibility is included, furthermore, the global fit would redetermine σ_0 and $C_{\rm sym}$. For simplicity, in the present qualitative analysis, we ignore such feedback corrections on σ_0 and $C_{\rm sym}$, which would have to be allowed for for more quantitative analysis. We remark in passing that $C_{\rm sym} = 1.9$ is also consistent with the empirical A dependence of the energy position of the giant dipole resonance [56].

We can now utilize the optimal values of C to examine how well the compressible droplet model can reproduce the neutron-skin thickness calculated from the HF+BCS model for Ca, Ni, Zr, Sn, Yb, and Pb isotopes. Here, we determine R_p, R, b_n, and b_p from the HF+BCS proton and neutron density distributions and then substitute the resultant values, together with the corresponding values of C and S_0, into the expressions for $\Delta r_{np}^{\rm vol}$ and $\Delta r_{np}^{\rm surf}$. The results from the three Skyrme interactions, SkM*, SLy4, and SkI3, are shown in Fig. 4. We also plot the decomposition of Δr_{np} into the volume and surface terms in the droplet model. The volume and surface contributions are found to be comparable for all the nuclides considered here. The volume term monotonically increases almost linearly with δ, whereas the surface term increases in such a way as to reflect the difference of the surface widths or diffuseness of protons and neutrons. As for SkM* and SLy4, not only large enhancement of Δr_{np} due to weakly bound orbits beyond the neutron magic numbers 28, 50, 82, and 126 for spherical Ca, Ni, Sn, and Pb isotopes, respectively, but also zigzag patterns for Zr isotopes, which stem from the nuclear deformation, are fairly well reproduced. Such reproduction of the local structure is ensured by the surface term. It is to be noted that, as far as the SkI3 interaction is concerned, the droplet results for Δr_{np} deviate considerably from the HF+BCS ones, for Pb isotopes in particular.

For the SkM* and SLy4 interactions, our macroscopic model fairly well reproduces Δr_{np} obtained by the HF+BCS calculations up to $\delta \sim 0.2$. Since the formula given by Eqs. (9) and (11) assumes $R_p \sim R_n$, higher order terms, which start with the quadratic term [23], should be considered for more quantitative description of the regime $\delta \gtrsim 0.2$.

To test the interaction dependence further, we display in Fig. 5 the same plot as Fig. 4 but for Sn and Pb isotopes with the KDE0v1, LNS, SkT1–3, and SV-sym32 interactions. The KDE0v1 and SV-sym32 interactions show a marginally good agreement of the macroscopic result for Δr_{np} with the microscopic one obtained by the HF+BCS calculations for

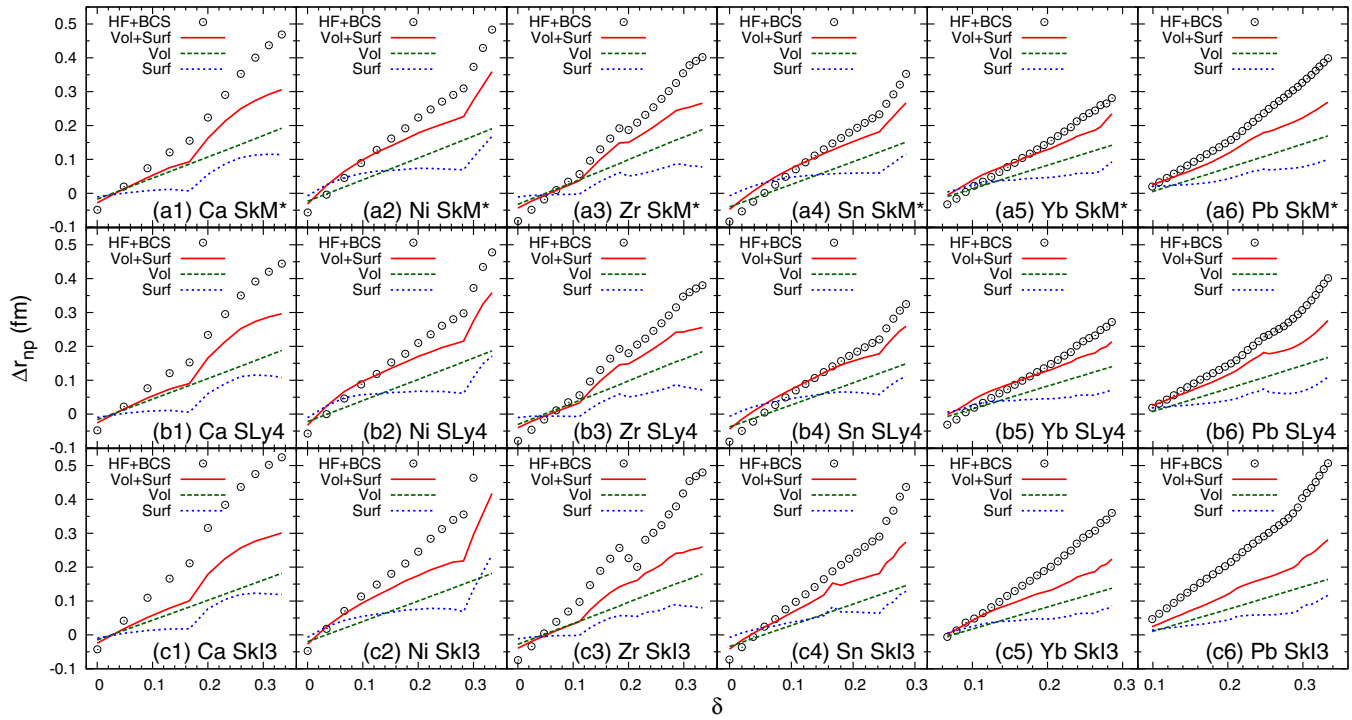

FIG. 4. Neutron-skin thickness of Ca, Ni, Zr, Sn, Yb, and Pb isotopes (from left to right, respectively) as a function of the asymmetry parameter $\delta = (N - Z)/A$. The SkM*, SLy4, and SkI3 interactions (from top to bottom, respectively) are employed for the HF+BCS calculations (circles) and for the droplet formula (solid lines) with the volume term (dashed lines) and the surface term (dotted lines).

Sn and Pb isotopes, while the LNS exhibits an appreciable difference between these two. The SkT1–3 interactions give a reasonable agreement, which is better for Pb isotopes than that for Sn isotopes.

Table I summarizes the EOS parameters, which are taken from Ref. [1], and the extracted χ values for various sets of the Skyrme interactions. Recall that the χ is correlated with the surface symmetry coefficient $C_{\rm sym}$. The smallest value of $C_{\rm sym}$ as assumed here is 1.4, which can be obtained from a Bethe-Weizsäecker type mass formula that includes the surface symmetry term. Then, we set $C_{\rm sym} = 1.9 \pm 0.5$, which in turn determines uncertainly in χ given that σ_0 is known much better.

TABLE I. EOS parameters derived from nine Skyrme-EDF models [1] and the density dependence of the surface tension, χ, that is consistent with the empirical C value. Units are given in fm^{-3} for ρ_0 and MeV for S_0, K_0, and L.

Name	ρ_0	S_0	K_0	L	χ ($C_{\rm sym} = 1.9 \mp 0.5$)
SkM*	0.160	30.03	216.61	45.78	1.16±0.79
SLy4	0.160	32.00	229.91	45.94	1.35±0.83
SkI3	0.158	34.83	258.19	100.53	0.76±0.43
KDE0v1	0.165	31.97	223.90	41.42	1.60±0.90
LNS	0.175	33.43	210.78	61.45	1.28±0.57
SkT1	0.161	32.02	236.16	56.18	1.15±0.70
SkT2	0.161	32.00	235.73	56.16	1.15±0.70
SkT3	0.161	31.50	235.74	55.31	1.14±0.71
SV-sym32	0.159	32.00	233.81	57.07	1.08±0.68

We remark that the surface pressure acts to enlarge (reduce) the nuclear size for $\chi \gtrsim (\lesssim) 2/3$ [23]. The values of χ obtained for the SkM* and SLy4 interactions are generally close to the Fermi-gas-model prediction $\chi = 4/3$. As an exception, the SkI3 interaction gives a considerably smaller χ, which reflects the fact that the corresponding EOS parameter L/K_0 is significantly larger than those of the other interactions.

Since K_0 is not strongly dependent on the Skyrme interaction employed, it is interesting to focus on the value of $L\chi$ for each of the Skyrme EDF models. The $L\chi$ values are 50–70 MeV for all the interactions except for the SkI3 and LNS interactions. These exceptional interactions give $L\chi > 70$ MeV, resulting in the poor reproduction of the microscopically obtained Δr_{np}. We remark that the EOS parameters of the SkI3 interaction are excluded in the constraint with the neutron-skin thickness of doubly closed nuclei [22] and also in the unitary gas constraint [57]. It should be noted that our analysis is based on the specific model, namely, nonrelativistic mean-field with the Skyrme effective interaction. Further investigation with other models, e.g., the relativistic mean-field model, would be desired to further confirm whether the finding obtained here is universal or not.

E. Effect of pairing on nuclear surface

Generally, the nuclear diffuseness reflects the structure around the nuclear surface, while the pairing correlation is known to play an essential role in a realistic description of the nuclear surface because it defines the occupations of single-particle states near the Fermi surface. Here we discuss

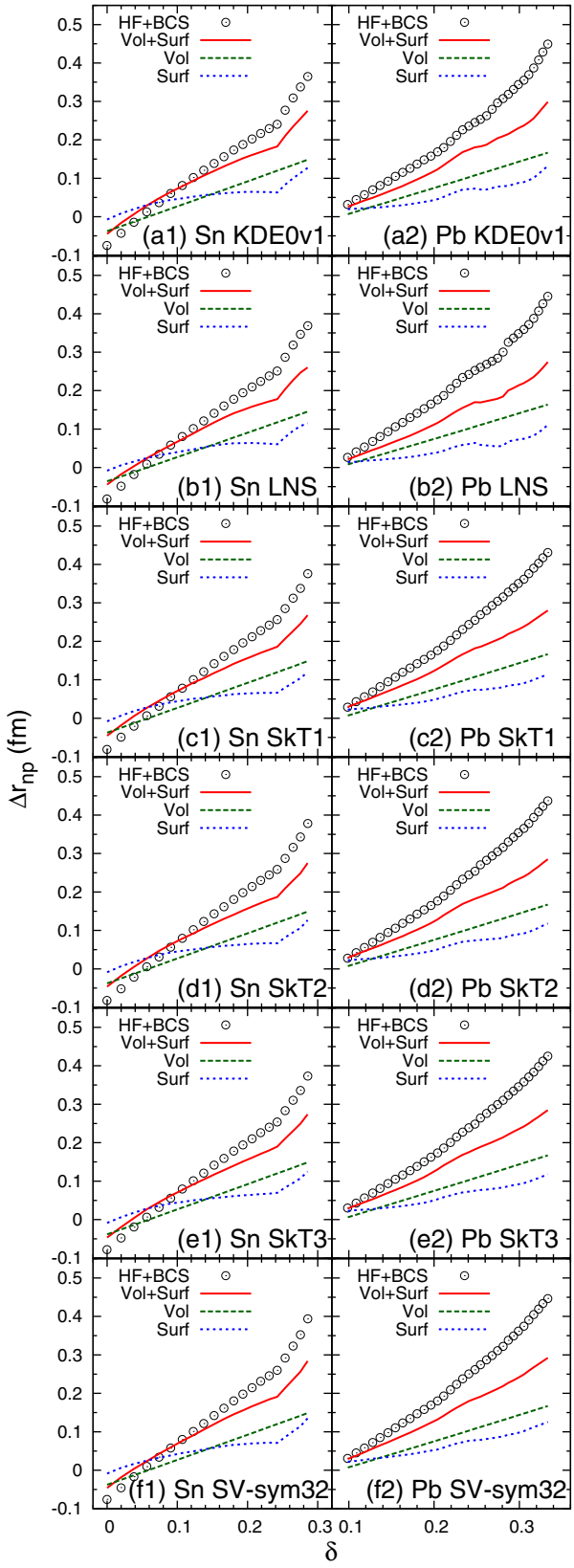

FIG. 5. Same as Fig. 4 but for (left) Sn and (right) Pb isotopes with the (a) KDE0v1, (b) LNS, (c) SkT1, (d) SkT2, (e) SkT3, and (f) SV-sym32 interactions.

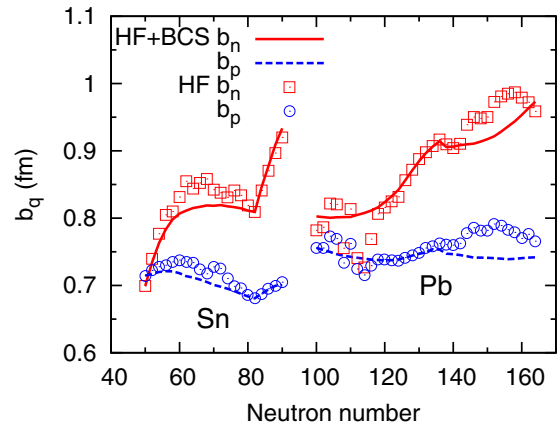

FIG. 6. Surface widths of Sn and Pb isotopes that are extracted from the neutron and proton density distributions calculated in the presence (HF+BCS) and absence (HF) of the pairing interaction. The SkM* interaction is employed for calculations of the density distributions.

the effect of the pairing correlation on the nuclear surface width of the density distributions obtained by the microscopic calculations.

Figure 6 plots the surface widths obtained from the density distributions of Sn and Pb isotopes that are calculated in the presence and absence of the pairing interaction. The surface widths tend to be large when the pairing interaction is ignored. In most cases, the pairing correlation plays a role in reducing the degree of the nuclear deformation. In fact, in the presence of the pairing interaction, all the Sn isotopes have a spherical shape, whereas the deformed ground states occur when the pairing interaction is off, resulting in such an artificial increase of the rms radii [17] as is not seen in the experimental charge radii [46]. At $N \geqslant 82$, on the other hand, a spherical shape is robust in both cases. All the Pb isotopes also show a spherical shape in the presence of the paring interaction. The effect appears to be small at $120 \lesssim N \lesssim 140$, in which the HF ground states have an almost spherical shape, while we see some difference at the neutron- and proton-rich regions where a large deformation appears in the HF ground states.

Figure 7 plots the surface correction term of Eq. (11) calculated by allowing for and ignoring the pairing interaction for Sn and Pb isotopes. Since both proton and neutron distributions are deformed, subtraction of the surface widths between protons and neutrons in Eq. (11) somewhat cancels the effect of the nuclear deformation. Although there is no significant difference between both cases, switch-off of the pairing interaction allows an artificial zigzag pattern, which is not seen in the experimental neutron-skin thickness [12,13], to appear in the surface correction term at the open shell regions. This suggests that the pairing interaction plays an important role in correctly describing the nuclear surface. In order to extract the EOS parameters from finite nuclei, therefore, detailed study on the effect of the paring correlation will be indispensable. In this paper, we employ a constant-monopole-type paring [31,32] as one of the standard paring interactions.

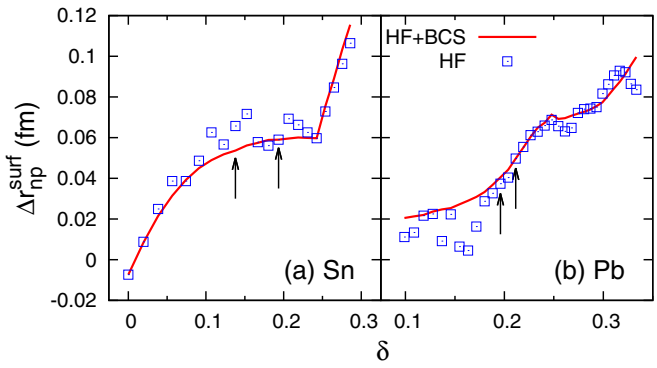

FIG. 7. Same as Fig. 6 but for the surface contribution to the neutron-skin thickness of (a) Sn and (b) Pb isotopes. To guide the eyes, arrows indicating the regions of $^{116-124}$Sn and $^{206-208}$Pb in which experimental data are available are drawn in panels (a) and (b), respectively.

Investigations with other types of the paring interaction would be interesting but are beyond the scope of this paper.

IV. CONCLUSIONS

In summary, to revisit a relation between the neutron skin thickness of finite nuclei and the EOS of asymmetric nuclear matter, we apply a compressible nuclear droplet model including an appropriate correction of the neutron and proton surfaces to a description of the neutron-skin thickness. This is a significant update of the previous work [23], which did not include any corrections due to the surface diffuseness. For several sets of the EOS parameters that correspond to the specific Skyrme effective interactions, we determine the density dependence of the surface tension, χ, in the nuclear droplet from empirical data for the neutron and proton density distributions of stable Sn and Pb isotopes. Such a determination provides possible way of determining the density dependence of the surface tension, which is a key quantity to bridge a gap between microscopic and macroscopic nuclear models.

We also present a reasonable definition of the surface width of the nuclear density distribution by using realistic density distributions of Ca, Ni, Zr, Sn, Yb, and Pb isotopes that are generated by the microscopic Skyrme Hartree-Fock (HF) + BCS model. We confirm from our macroscopic model that the difference of the proton and neutron surface widths plays a decisive role in determining the neutron-skin thickness. In fact, the surface width correction to the thickness can be comparable to the volume contribution, which contains information on the bulk properties of nuclear matter. This seems to be one of the reasons why the parameter L characterizing the density dependence of the symmetry energy, which does have a strong correlation with the skin thickness, is still uncertain.

Another reason for that could be uncertainties in the surface tension, which, together with the bulk properties, controls the volume contribution. Even with χ being determined in the present analysis, the surface symmetry coefficient $C_{\rm sym}$ has yet to be precisely fixed by experimental data.

Fortunately, we still have some chance of constraining the EOS parameters. This is based on the consistency check of the thermodynamic droplet description of the neutron skin thickness with the HF+BCS prediction for each of the Skyrme interactions adopted here. We find most of the Skyrme interactions have χ of the order of the Fermi-gas value $4/3$. In particular, the SkM* and SLy4 interactions show an almost perfect consistency between the microscopically and macroscopically obtained neutron-skin thickness. A group with $L\chi \sim 50$–70 MeV, in which the SkM* and SLy4 interactions are included, shows a good consistency, in contrast to a group with $L\chi \gtrsim 70$ MeV. This implies that the latter group is not thermodynamically favored, although a more quantitative analysis that allows for shell and pairing effects on the primary factor C would be desired to make sure of that.

To obtain a better constraint on the EOS parameters, systematic investigations on the surface diffuseness of nuclei, including neutron-rich unstable ones, would be necessary. The surface width or diffuseness of unstable nuclei could be experimentally determined, e.g., by using elastic scattering in inverse kinematics with a proton target. Such measurements would be hopefully made in the near future to deepen our understanding of asymmetric nuclear matter.

ACKNOWLEDGMENTS

We thank S. Terashima for sending us the numerical data of proton and neutron density distributions of Sn isotopes. We are also grateful to J. M. Lattimer for valuable communications. Computational resources were in part provided by the Research Center for Nuclear Physics, Osaka University. This work was performed in part at the Aspen Center for Physics, which is supported by NSF Grant No. PHY-1607611. Also, this work was supported in part by Grants-in-Aid for Scientific Research on Innovative Areas through No. 24105008 provided by MEXT.

[1] M. Dutra, O. Lourenço, J. S. Sá Martins, A. Delfino, J. R. Stone, and P. D. Stevenson, Phys. Rev. C **85**, 035201 (2012).
[2] P. B. Demorest, T. Pennucci, S. M. Ransom, M. S. E. Roberts, and J. W. T. Hessels, Nature (London) **467**, 1081 (2010).
[3] L. W. Chen, C. M. Ko, B. A. Li, and J. Xu, Phys. Rev. C **82**, 024321 (2010).
[4] P.-G. Reinhard and W. Nazarewicz, Phys. Rev. C **81**, 051303(R) (2010).
[5] X. Roca-Maza, M. Centelles, X. Viñas, and M. Warda, Phys. Rev. Lett. **106**, 252501 (2011).
[6] M. Kortelainen, J. Erler, W. Nazarewicz, N. Birge, Y. Gao, and E. Olsen, Phys. Rev. C **88**, 031305(R) (2013).
[7] T. Inakura, T. Nakatsukasa, and K. Yabana, Phys. Rev. C **88**, 051305(R) (2013).
[8] X. Roca-Maza, X. Viñas, M. Centelles, B. K. Agrawal, G. Coló, N. Paar, J. Piekarewicz, and D. Vretenar, Phys. Rev. C **92**, 064304 (2015).
[9] H. de Vries, C. W. Jager, and C. de Vries, At. Data Nucl. Data Tables **36**, 495 (1987).
[10] S. Abrahamyan *et al.*, Phys. Rev. Lett. **108**, 112502 (2012).

[11] Proposal to Jefferson Lab PAC 38, available at http://hallaweb.jlab.org/parity/prex/prexII.pdf.

[12] S. Terashima, H. Sakaguchi, H. Takeda, T. Ishikawa, M. Itoh, T. Kawabata, T. Murakami, M. Uchida, Y. Yasuda, M. Yosoi, J. Zenihiro, H. P. Yoshida, T. Noro, T. Ishida, S. Asaji, and T. Yonemura, Phys. Rev. C **77**, 024317 (2008).

[13] J. Zenihiro, H. Sakaguchi, T. Murakami, M. Yosoi, Y. Yasuda, S. Terashima, Y. Iwao, H. Takeda, M. Itoh, H. P. Yoshida, and M. Uchida, Phys. Rev. C **82**, 044611 (2010).

[14] K. Tanaka, T. Yamaguchi, T. Suzuki, T. Ohtsubo, M. Fukuda, D. Nishimura, M. Takechi, K. Ogata, A. Ozawa, T. Izumikawa, T. Aiba, N. Aoi, H. Baba, Y. Hashizume, K. Inafuku, N. Iwasa, K. Kobayashi, M. Komuro, Y. Kondo, T. Kubo, M. Kurokawa, T. Matsuyama, S. Michimasa, T. Motobayashi, T. Nakabayashi, S. Nakajima, T. Nakamura, H. Sakurai, R. Shinoda, M. Shinohara, H. Suzuki, E. Takeshita, S. Takeuchi, Y. Togano, K. Yamada, T. Yasuno, and M. Yoshitake, Phys. Rev. Lett. **104**, 062701 (2010).

[15] T. Moriguchi, A. Ozawa, S. Ishimoto, Y. Abe, M. Fukuda, I. Hachiuma, Y. Ishibashi, Y. Ito, T. Kuboki, M. Lantz, D. Nagae, K. Namihira, D. Nishimura, T. Ohtsubo, H. Ooishi, T. Suda, H. Suzuki, T. Suzuki, M. Takechi, K. Tanaka, and T. Yamaguchi, Phys. Rev. C **88**, 024610 (2013).

[16] W. Horiuchi, Y. Suzuki, and T. Inakura, Phys. Rev. C **89**, 011601(R) (2014).

[17] W. Horiuchi, S. Hatakeyama, S. Ebata, and Y. Suzuki, Phys. Rev. C **93**, 044611 (2016).

[18] A. Estradé, R. Kanungo, W. Horiuchi, F. Ameil, J. Atkinson, Y. Ayyad, D. Cortina-Gil, I. Dillmann, A. Evdokimov, F. Farinon, H. Geissel, G. Guastalla, R. Janik, M. Kimura, R. Knobel, J. Kurcewicz, Y. A. Litvinov, M. Marta, M. Mostazo, I. Mukha, C. Nociforo, H. J. Ong, S. Pietri, A. Prochazka, C. Scheidenberger, B. Sitar, P. Strmen, Y. Suzuki, M. Takechi, J. Tanaka, I. Tanihata, S. Terashima, J. Vargas, H. Weick, and J. S. Winfield, Phys. Rev. Lett. **113**, 132501 (2014).

[19] S. Terashima *et al.*, Prog. Theor. Exp. Phys. **2014**, 101D02 (2014).

[20] Y. Suzuki, W. Horiuchi, S. Terashima, R. Kanungo, F. Ameil, J. Atkinson, Y. Ayyad, D. Cortina-Gil, I. Dillmann, A. Estrade, A. Evdokimov, F. Farinon, H. Geissel, G. Guastalla, R. Janik, R. Knoebel, J. Kurcewicz, Y. A. Litvinov, M. Marta, M. Mostazo, I. Mukha, C. Nociforo, H. J. Ong, S. Pietri, A. Prochazka, C. Scheidenberger, B. Sitar, P. Strmen, M. Takechi, J. Tanaka, I. Tanihata, J. Vargas, H. Weick, and J. S. Winfield, Phys. Rev. C **94**, 011602(R) (2016).

[21] R. Kanungo, W. Horiuchi, G. Hagen, G. R. Jansen, P. Navratil, F. Ameil, J. Atkinson, Y. Ayyad, D. Cortina-Gil, I. Dillmann, A. Estrade, A. Evdokimov, F. Farinon, H. Geissel, G. Guastalla, R. Janik, M. Kimura, R. Knobel, J. Kurcewicz, Y. A. Litvinov, M. Marta, M. Mostazo, I. Mukha, C. Nociforo, H. J. Ong, S. Pietri, A. Prochazka, C. Scheidenberger, B. Sitar, P. Strmen, Y. Suzuki, M. Takechi, J. Tanaka, I. Tanihata, S. Terashima, J. Vargas, H. Weick, and J. S. Winfield, Phys. Rev. Lett. **117**, 102501 (2016).

[22] B. A. Brown, Phys. Rev. Lett. **111**, 232502 (2013).

[23] K. Iida and K. Oyamatsu, Phys. Rev. C **69**, 037301 (2004).

[24] M. Yamada, Prog. Theor. Phys. **32**, 512 (1964).

[25] M. Warda, X. Viñas, X. Roca-Maza, and M. Centelles, Phys. Rev. C **80**, 024316 (2009).

[26] J. M. Lattimer, Annu. Rev. Nucl. Part. Sci. **31**, 337 (1981).

[27] W. D. Myers and W. J. Swiatecki, Ann. Phys. (NY) **55**, 395 (1969); **84**, 186 (1974).

[28] E. Hilf and G. Süssmann, Phys. Lett. **21**, 654 (1966).

[29] A. Bohr and B. R. Mottelson, *Nuclear Structure* (W. A. Benjamin, New York, 1975), Vol. I.

[30] A. Kohama, K. Iida, and K. Oyamatsu, J. Phys. Soc. Jpn. **85**, 094201 (2016).

[31] S. Ebata, T. Nakatsukasa, and T. Inakura, Phys. Rev. C **90**, 024303 (2014).

[32] S. Ebata and T. Nakatsukasa, Phys. Scr. **92**, 064005 (2017).

[33] S. Ebata, T. Nakatsukasa, T. Inakura, K. Yoshida, Y. Hashimoto, and K. Yabana, Phys. Rev. C **82**, 034306 (2010).

[34] W. Horiuchi, T. Inakura, T. Nakatsukasa, and Y. Suzuki, Phys. Rev. C **86**, 024614 (2012).

[35] R. J. Glauber, in *Lectures in Theoretical Physics*, edited by W. E. Brittin and L. G. Dunham (Interscience, New York, 1959), Vol. 1, p. 315.

[36] W. Horiuchi, T. Inakura, T. Nakatsukasa, and Y. Suzuki, JPS Conf. Proc. **6**, 030079 (2015).

[37] M. Takechi *et al.*, Mod. Phys. Lett. A **25**, 1878 (2010).

[38] M. Takechi *et al.*, Phys. Rev. C **90**, 061305(R) (2014).

[39] J. Bartel, P. Quentin, M. Brack, C. Guet, and H. Håkansson, Nucl. Phys. A **386**, 79 (1982).

[40] E. Chabanat, P. Bonche, P. Haensel, J. Meyer, and R. Schaeffer, Nucl. Phys. A **627**, 710 (1997).

[41] P.-G. Reinhard and H. Flocard, Nucl. Phys. A **584**, 467 (1995).

[42] B. K. Agrawal, S. Shlomo, and V. K. Au, Phys. Rev. C **72**, 014310 (2005).

[43] L. G. Cao, U. Lombardo, C. W. Shen, and N. V. Giai, Phys. Rev. C **73**, 014313 (2006).

[44] F. Tondeur, M. Brack, M. Farine, and J. M. Pearson, Nucl. Phys. A **420**, 297 (1984).

[45] P. Klúpfel, P.-G. Reinhard, T. J. Bürvenich, and J. A. Maruhn, Phys. Rev. C **79**, 034310 (2009).

[46] I. Angeli and K. P. Marinova, At. Data Nucl. Data Tables **99**, 69 (2013).

[47] J. L. Friar, J. Martorell, and D. W. L. Sprung, Phys. Rev. A **56**, 4579 (1997).

[48] P. M. Goddard, P. D. Stevenson, and A. Rios, Phys. Rev. Lett. **110**, 032503 (2013).

[49] K. Minomo, T. Sumi, M. Kimura, K. Ogata, Y. R. Shimizu, and M. Yahiro, Phys. Rev. C **84**, 034602 (2011).

[50] K. Minomo, T. Sumi, M. Kimura, K. Ogata, Y. R. Shimizu, and M. Yahiro, Phys. Rev. Lett. **108**, 052503 (2012).

[51] T. Sumi, K. Minomo, S. Tagami, M. Kimura, T. Matsumoto, K. Ogata, Y. R. Shimizu, and M. Yahiro, Phys. Rev. C **85**, 064613 (2012).

[52] S. Watanabe, K. Minomo, M. Shimada, S. Tagami, M. Kimura, M. Takechi, M. Fukuda, D. Nishimura, T. Suzuki, T. Matsumoto, Y. R. Shimizu, and M. Yahiro, Phys. Rev. C **89**, 044610 (2014).

[53] W. Horiuchi, S. Hatakeyama, S. Ebata, and Y. Suzuki, Phys. Rev. C **96**, 024605 (2017).

[54] K. Oyamatsu and K. Iida, Prog. Theor. Phys. **109**, 631 (2003).

[55] H. Koura, T. Tachibana, M. Uno, and M. Yamada, Prog. Theor. Phys. **113**, 305 (2005).

[56] L. Trippa, G. Coló, and E. Vigezzi, Phys. Rev. C **77**, 061304 (2008).

[57] I. Tews, J. M. Lattimer, A. Ohnishi, and E. E. Kolomeitsev, arXiv:1611.07133v2.